Available online at www.sciencedirect.com

ScienceDirect

Journal of Magnesium and Alloys 11 (2023) 991–997

www.elsevier.com/locate/jma

Full Length Article

Remarkably slow corrosion rate of high-purity Mg microalloyed with 0.05wt% Sc

Soo-Min Baek, Jeong-Ki Kim, Du-Won Min, Sung Soo Park*

Department of Materials Science and Engineering, Ulsan National Institute of Science and Technology, Ulsan 44919, Republic of Korea

Received 13 April 2022; received in revised form 27 June 2022; accepted 18 August 2022
Available online 28 September 2022

Abstract

We report that the corrosion resistance of Mg is significantly improved by adding 0.05wt% Sc. Corrosion rates evaluated from weight loss values after room-temperature immersion in 0.6 M NaCl solution for two weeks were 0.27 and 4.0 mm y^{-1} for the high-purity Mg samples with and without microalloyed 0.05wt% Sc, respectively. The beneficial effect of Sc microalloying on the corrosion resistance of Mg is discussed in connection with Sc-induced microstructural modifications.

Keywords: Magnesium; Microalloying; Intermetallic phase; Microgalvanic corrosion.

1. Introduction

Metallic materials have a surficial oxide layer, which can act as a barrier to degradation in a corrosive environment [1–7]. The outstanding corrosion resistance of Ti and Al alloys is predominantly due to the protective role of the oxide layer [1–5]. On the other hand, the oxide layer of some metallic elements such as Fe and Mg does not inherently have sufficient protectiveness, resulting in their poor corrosion resistance [8–11]. In the case of Fe, however, this corrosion issue has been successfully resolved by alloying it with more than ∼11wt% Cr and currently a series of stainless steels with additional alloying elements are available for many applications where corrosion resistance is primarily required [7].

Unfortunately, however, the method in common use for Fe cannot be readily applied to Mg since the solid solubility of an element such as Cr, which can contribute to the formation of protective oxide layer, is limited in the Mg matrix. In these circumstances, artificial surface coating by anodizing or plasma electrolytic oxidation has been used to diminish the corrosion-induced degradation of Mg-based products [12–21]. Since it is quite difficult to acquire an initially defect-free coating layer and because the coating layer is susceptible to damage in practical use, localized corrosion is usually unavoidable. This suggests that the corrosion resistance of a base material underneath the protective layer is still important, regardless of the anti-corrosive performance of surface coatings.

Recently, it has been shown that the corrosion resistance of Mg alloys can be significantly enhanced by microalloying, which can lower the degree of microgalvanic reaction between the Mg matrix and adjacent secondary phases without appreciably improving the protectiveness of surficial oxide layer [22–35]. Among typically available alloying elements for Mg, rare-earth elements have been reported to be effective in terms of inactivating the microgalvanic corrosion of multi-phase Mg alloys [22–24,27–34].

The occurrence of microgalvanic corrosion is not wholly confined to alloy type materials since even high-purity Mg (HP-Mg) is usually found to have secondary phase particles, which contain impurities such as Fe and Si [10,36–39]. The problematic influence of these impurity-bearing particles on corrosion resistance is not to be ignored, especially considering their electrochemically noble character relative to Mg [10,37–39]. Despite the inevitable risk of raising production

---

* Corresponding author.
E-mail address: sspark@unist.ac.kr (S.S. Park).

https://doi.org/10.1016/j.jma.2022.08.003

Table 1
Analyzed chemical compositions of the HP-Mg and Mg–0.05Sc samples investigated in this study.

Sample	Sc	Fe	Si	Mn	Ca	Mg
HP-Mg	<0.0001	0.0029	0.0047	0.012	0.028	bal.
Mg–0.05Sc	0.0506	0.0043	0.0065	0.013	0.030	bal.

cost, researchers have sought to produce ultra-high-purity Mg (UHP-Mg) to circumvent the corrosion acceleration problem in the presence of particles containing impurities and to date a very slow corrosion rate of ∼0.25 mm y^{-1} has been reported for UHP-Mg immersed in a 0.6 M NaCl solution [36]. Aside from the research activities related to UHP-Mg, it has been also shown that alloying with elements such as As, Ge, or Ca is effective in enhancing the corrosion resistance of pure Mg [35,40,41]. Here, as an alternative alloying method, we report that achieving corrosion resistance comparable to UHP-Mg is readily possible by a trace addition of 0.05wt% Sc to HP-Mg. In this study, HP-Mg samples with and without microalloyed Sc were subjected to an equal preparation method and then their microstructure and corrosion behavior were comparatively investigated.

2. Experimental procedure

The analyzed compositions (wt%) of HP-Mg and Mg–0.05Sc samples are provided in Table 1. The Mg samples were prepared by induction melting under purging of inert gases of CO_2 and SF_6. Each sample in the molten state was stabilized at 750 °C for 10 minutes and then poured into a steel mold preheated to 200 °C. The dimensions of cast samples were 12 mm in thickness, 50 mm in width, and 100 mm in height. Microstructural examinations were conducted by an EPIPHOT 200 optical microscope (OM), a Quanta 200 field-emission scanning electron microscope (SEM) with an EDAX Apollo X energy dispersive spectrometer (EDS), and a JEM-2100F transmission electron microscope (TEM). Quanta 3D FEG focused ion beam equipment was used to prepare TEM samples.

The corrosion rates of the HP-Mg and Mg–0.05Sc samples were measured by room-temperature immersion tests in a 0.6 M NaCl solution for up to two weeks. Cuboidal samples with a side length of 10 mm were immersed in a solution whose temperature was kept constant at 25 °C. According to ASTM G1-03, the samples after immersion were directly soaked in 200 g l^{-1} CrO_3 solution at 50 °C for 10 minutes to remove oxidized corrosion products and then weight loss was measured. During the immersion tests, evolved H_2 volume was measured according to the method reported by Song and Atrens [10].

To compare the electrochemical potential differences between the Mg matrix and secondary phase particles, Volta potential distribution was examined by scanning Kelvin probe force microscopy (SKPFM) with an NTEGRA atomic force microscope. The SKPFM measurements were performed in atmospheric conditions under a controlled relative humidity of 40 ± 5% at 25 °C. Potentiodynamic polarization tests and electrochemical impedance spectroscopy (EIS) measurements were performed by a Reference 600 potentiostat after immersion for three days in a 0.6 M NaCl solution at 25 °C after deaeration with N_2 gas. The polarization curve of each sample was obtained from -0.3 V_{SCE} to film breakdown and the potential scan rate was 1 mV s^{-1}. A conventional three-electrode cell was used with a saturated calomel reference electrode (SCE), a Pt counter electrode, and a working electrode (sample). The scan frequency for the Nyquist plots from the EIS measurements ranged from 100 kHz to 10 mHz with a perturbation amplitude of ∼10 mV.

3. Results and discussion

Fig. 1 shows the appearances and surface conditions of the HP-Mg and Mg–0.05Sc samples after immersion for two weeks in the 0.6 M NaCl solution. As can be seen in the OM micrographs and corresponding micro-CT images, the HP-Mg sample was severely damaged under the corrosive condition whereas the Mg–0.05Sc sample retained its original rectangular shape with only shallow and spotty degradation. The SEM micrographs revealed that the depths of oxide scales penetrating the base metal parts approach ∼400 μm and ∼10 μm for the HP-Mg and Mg–0.05Sc samples, respectively. The oxide scales on HP-Mg were found to contain defects or void parts while such imperfections were not easily detected in the case of Mg–0.05Sc, which appeared to corrode far more uniformly. Weight loss values of the HP-Mg and Mg–0.05Sc samples after two weeks in the 0.6 M NaCl solution measured 26.6 ± 1.0 and 1.6 ± 0.2 mg cm^{-2}, which correspond to corrosion rates of 4.0 ± 0.1 and 0.27 ± 0.03 mm y^{-1}, respectively. It is remarkable that such a small addition of Sc to HP-Mg can lead to a decrease of its corrosion rate by ∼93%. As represented in Fig. 2a, weight-loss-based corrosion rates after three days in the 0.6 M NaCl solution were 4.9 ± 0.6 and 0.36 ± 0.03 mm y^{-1} for the HP-Mg and Mg–0.05Sc samples, respectively. It should be noted here that the corrosion rates of 0.27∼0.36 mm y^{-1} obtained in this study are much slower than the previously reported corrosion rates of 1∼2 mm y^{-1} in the Mg samples containing 0.1∼5wt% Sc [42–44], suggesting that the optimum Sc content for the corrosion resistance of Mg has not been properly explored yet. Analogous to the immersion test results, there appeared clear differences in H_2 evolution volume between the two samples with different Sc content, as shown in Fig. 2b.

The SEM micrographs given in Fig. 3 show that the microstructures of the two Mg samples with different Sc content can be characterized by the type of second-phase particles, which are sparsely dotted in the α-Mg matrix. It can be seen that the HP-Mg sample has small cuboidal particles with sizes under ∼200 nm while the Mg–0.05Sc sample contains somewhat longish particles a little larger in size as compared to those in HP-Mg. TEM-EDS analysis indicated that these particles in HP-Mg and Mg–0.05Sc mainly contain Fe and Si, which exist as impurities in the samples. It can be also seen that Sc constitutes the particles in Mg–0.05Sc,

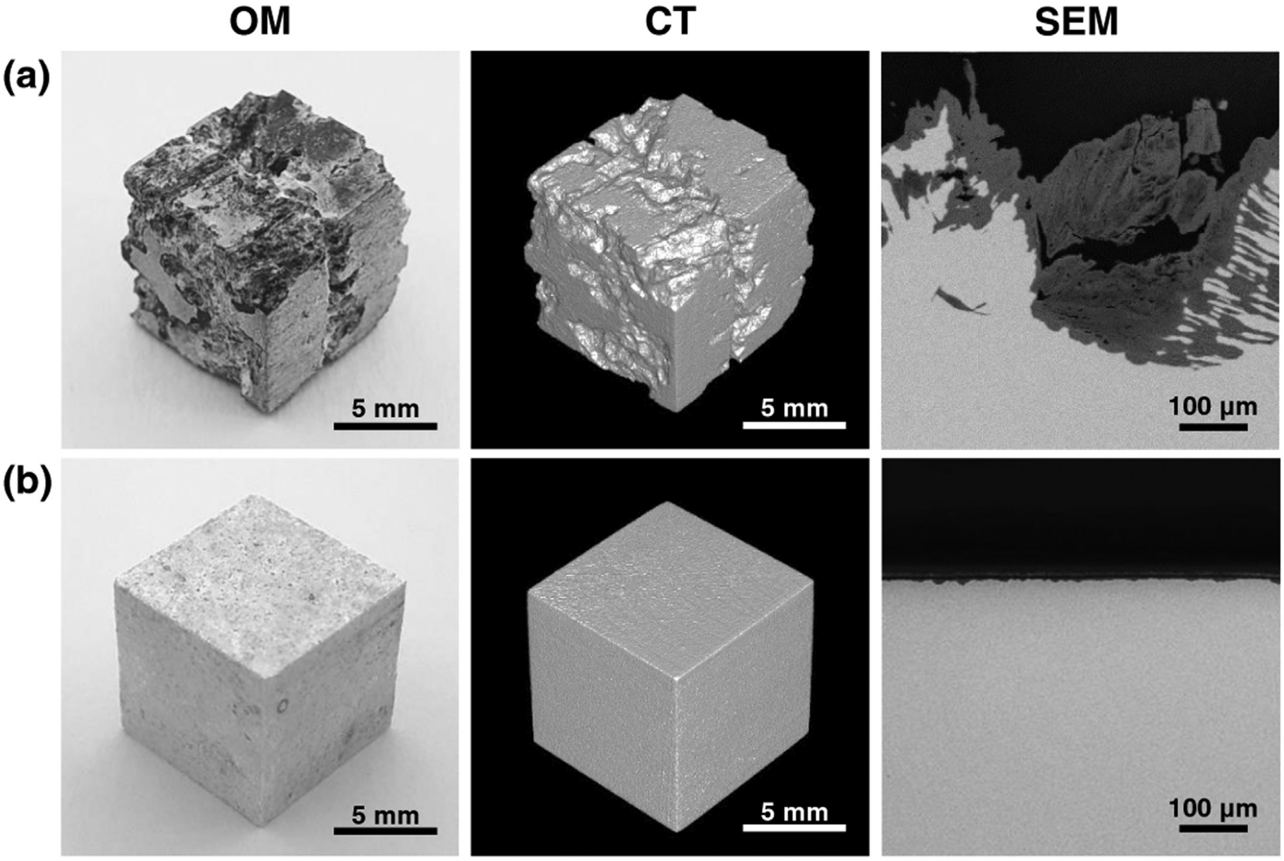

Fig. 1. Optical micrographs, corresponding micro-CT images, and low-magnification cross-sectional SEM micrographs of the (a) HP-Mg and (b) Mg–0.05Sc samples after immersion in 0.6 M NaCl solution for two weeks.

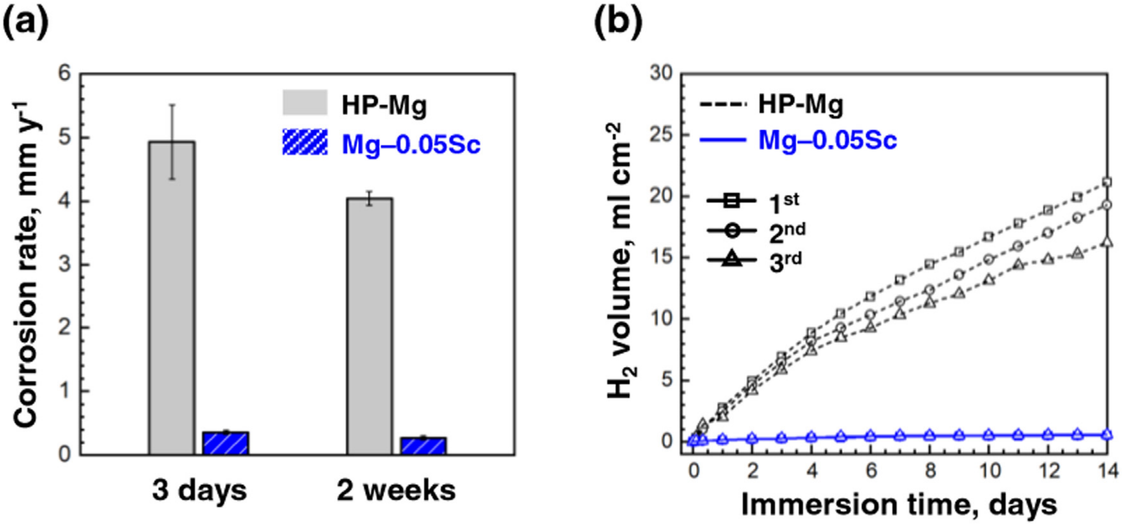

Fig. 2. (a) Weight-loss-based corrosion rate values of the HP-Mg and Mg–0.05Sc samples after immersion in 0.6 M NaCl solution for three days and two weeks and (b) evolved H_2 volume values of the HP-Mg and Mg–0.05Sc samples as a function of immersion time for up to 14 days in 0.6 M NaCl solution.

suggesting that the type of particles incorporating impurities in HP-Mg was changed by Sc microalloying. A TEM diffraction analysis confirmed that the particles in the HP-Mg and Mg–0.05Sc samples have different crystal structures and they were identified as face-centered cubic Fe_3Si and orthorhombic $ScFeSi_2$, respectively. Metallographic observations in Fig. S1 indicated that the two samples have grain sizes of ~350 μm and there is no clear difference in grain size between them.

Since the degree of microgalvanic corrosion between constituting phases is considered a decisive factor affecting the

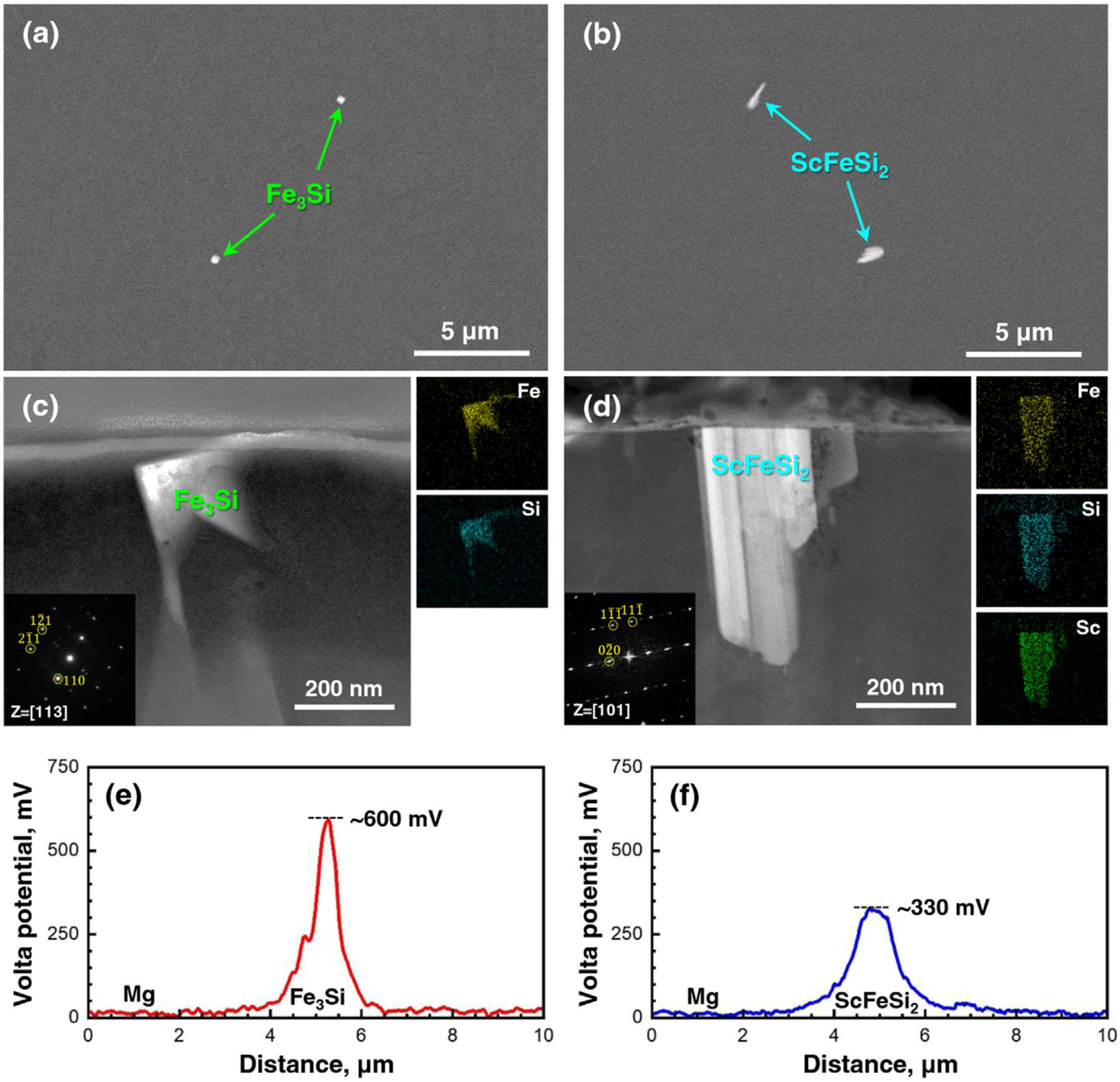

Fig. 3. SEM micrographs of the (a) HP-Mg and (b) Mg–0.05Sc samples, TEM micrographs of the (c) HP-Mg and (d) Mg–0.05Sc samples with the diffraction patterns and EDS maps, and Volta potential profiles obtained at the sample surfaces including (e) Fe_3Si and (f) $ScFeSi_2$ phases.

overall corrosion behavior of Mg alloys in a corrosive environment, different types of particles were subjected to a SKPFM analysis. As provided in Fig. 3 as well, the Volta potential values obtained by SKPFM were found to be ∼600 and ∼330 mV for the Fe_3Si particles in HP-Mg and the $ScFeSi_2$ particles in Mg–0.05Sc, respectively. This indicates that the particles containing Sc are much less noble than the particles typically observable in HP-Mg, suggestive of a reduced degree of microgalvanic corrosion in the Mg–0.05Sc sample.

Fig. 4 shows SEM micrographs and corresponding EDS maps of the HP-Mg and Mg–0.05Sc samples after immersion in the 0.6 M NaCl solution for one hour. Surficial changes were found to selectively occur in the vicinity of secondary particles, suggesting the operation of microgalvanic corrosion. The HP-Mg samples exhibited the formation of oxide scales and hollow pits at regions around Fe_3Si. SEM-EDS mapping indicated that the hollow pits correspond to the areas with relatively intense Cl signals. This can be understood by the attraction of Cl^- ions toward the hollow pits where Mg^{2+} ions actively generate during Mg dissolution [45–47]. By contrast, such significant changes visible in HP-Mg were not observed on the surface of Mg–0.05Sc and only a shallow dome-like oxide was detected at areas near $ScFeSi_2$ in the Sc-microalloyed sample. This indicates that microgalvanic corrosion between the Mg matrix and secondary phase particles was relatively more sluggish in Mg–0.05Sc where $ScFeSi_2$ particles emerged instead of Fe_3Si particles.

Fig. 5a shows the potentiodynamic polarization curves of the HP-Mg and Mg–0.05Sc samples after immersion in the 0.6 M NaCl solution for three days. First, the cathodic current density ($i_{cathodic}$) of Mg–0.05Sc is considerably lower than that of HP-Mg in the applied potential range. The average $i_{cathodic}$ values at -1.7 V_{SCE} were -0.163 ± 0.010 and -0.027 ± 0.007 mA cm^{-2} for the HP-Mg and Mg–0.05Sc samples, respectively. In addition, a significant difference in anodic polarization behavior can be seen between the two

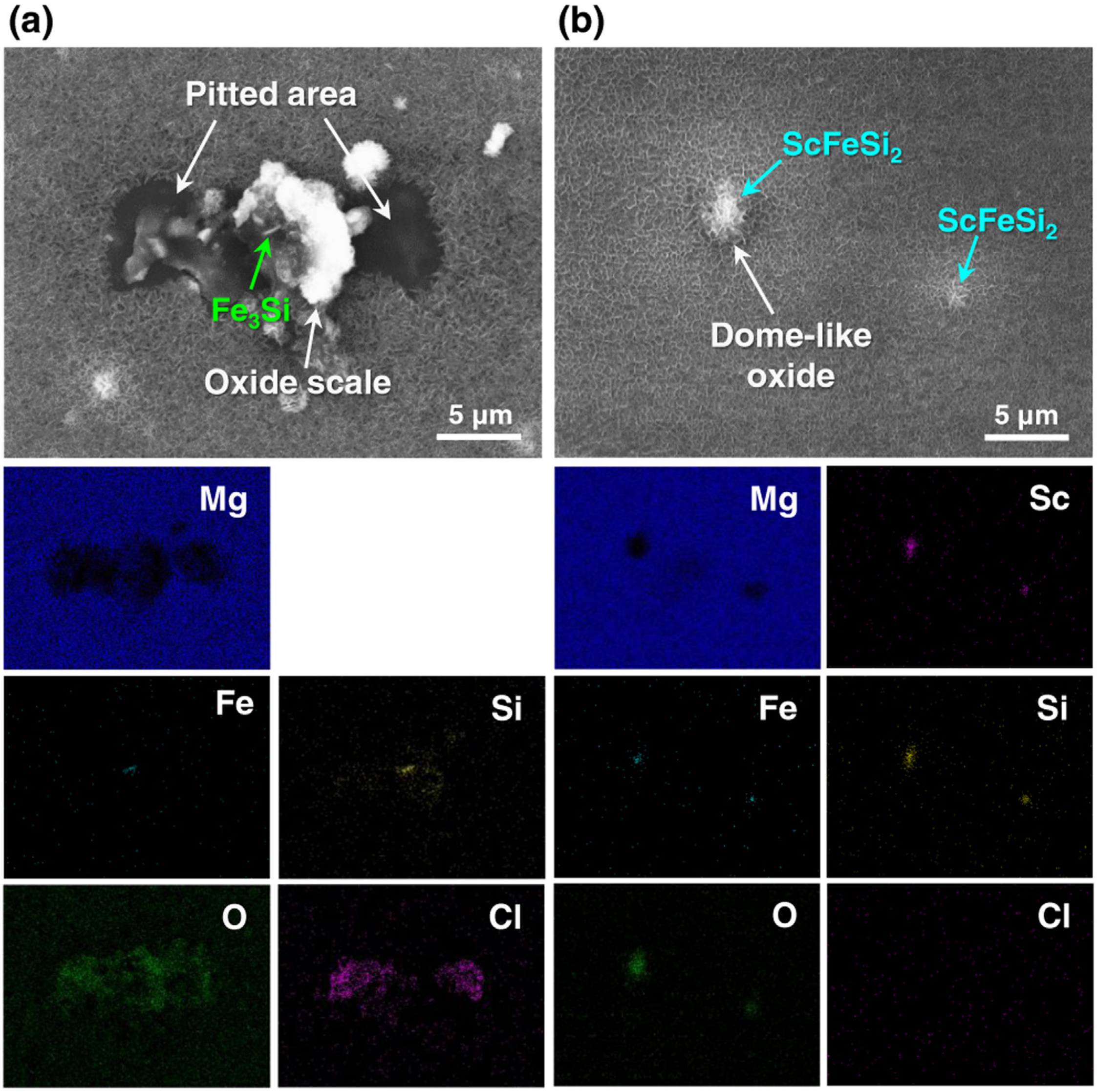

Fig. 4. SEM micrographs of the (a) HP-Mg and (b) Mg–0.05Sc samples after immersion in 0.6 M NaCl solution for one hour with corresponding EDS maps for elements of Mg, Fe, Si, O, Cl, or Sc.

samples. The Mg–0.05Sc sample represented passive behavior within a potential range of ~0.3 V from its corrosion potential whereas the HP-Mg sample did not clearly show passivity. The passive current density values at -1.5 V_{SCE} were 0.150 ± 0.047 and 0.015 ± 0.001 mA cm^{-2} for the HP-Mg and Mg–0.05Sc samples, respectively. These results indicate that the cathodic and anodic polarization behavior of HP-Mg was significantly affected by Sc microalloying.

Nyquist plots of the HP-Mg and Mg–0.05Sc samples are also presented in Fig. 5b. In the case of HP-Mg, spectra are composed of a high-frequency capacitive loop and a low-frequency inductive loop. By contrast, both high-frequency and medium-frequency capacitive loops were clearly observed in Mg–0.05Sc. The charge transfer resistance values, equivalent to the intersections of the high-frequency capacitive loops with the real Z-axis, were found to be 295 ± 41 and 3489 ± 403 Ohm cm^2 for the HP-Mg and Mg–0.05Sc samples, respectively, suggesting that these samples have considerably different dissolution rates of α-Mg in the corrosive condition.

The present study shows that the corrosion rate of HP-Mg in an aqueous NaCl solution can approach that of UHP-Mg by a trace addition of Sc. After immersion in 0.6 M NaCl solution for two weeks, HP-Mg with microalloyed 0.05wt% Sc exhibited a weight-loss-based corrosion rate of 0.27 mm y^{-1}, which is about 15 times slower than that of unalloyed HP-Mg. An electrochemical analysis revealed that the Sc-induced improvement of the corrosion resistance is a combined result of reduction of both the cathodic and anodic reaction rates in the corrosive medium. Microscopic observations at the early stage of corrosion indicated that the degree of microgalvanic corrosion between the anodic Mg and surrounding particulate cathodic phases was significantly diminished in the presence of $ScFeSi_2$ phase in Mg–0.05Sc instead of the nobler Fe_3Si

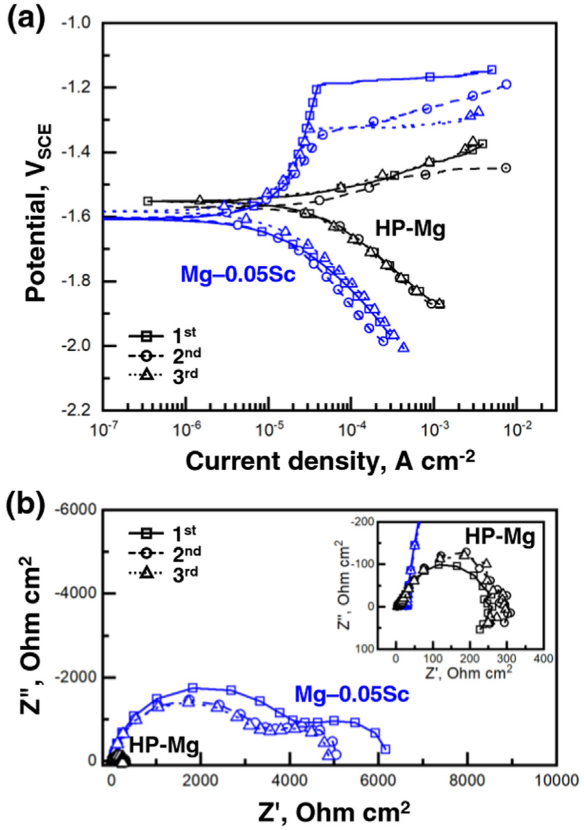

Fig. 5. (a) Potentiodynamic polarization curves and (b) Nyquist plots of the HP-Mg and Mg–0.05Sc samples after immersion in 0.6 M NaCl solution for three days.

phase in HP-Mg. This phase change toward lower electrochemical nobility due to micro-addition of Sc is responsible for the retardation of the cathodic H_2 evolution reaction, as shown in Fig. 2b.

With regard to the anodic reaction, its reaction rate is mainly affected by the intrinsic protectiveness of the surficial passive layer as well as defect formation on the layer. If there were no defect formation on the passive layer in both cases of HP-Mg and Mg–0.05Sc, the relatively retarded anodic reaction rate in the latter could be understood by enhanced protectiveness of the passive layer possibly incorporating oxides containing Sc. As shown in Figs. 1 and 4, however, only the HP-Mg sample showed numerous surface defects induced by microgalvanic corrosion, indicating that in this situation the intrinsic protectiveness of the passive layer cannot be simply compared between the two samples. Another aspect to consider is that the Sc content added to HP-Mg in this study is considered too small to be sufficiently influential and to account for the anodic branch of the potentiodynamic polarization curves. Thus, it should be noted here that the retardation of the anodic reaction after Sc microalloying was influenced by the presence of the relatively defect-free oxide layer on the surface, which can better protect the underlying metallic region. Such formation of the sound oxide layer after Sc microalloying is similar to the case of UHP-Mg where microgalvanic corrosion is minimized [36]. This means that changing the phase types toward lower electrochemical nobility also contributed to lowering of the anodic Mg dissolution rate by suppressing defect formation on the passive oxide layer, resulting in relatively uniform corrosion behavior in the HP-grade Sc-microalloyed Mg.

4. Conclusion

The corrosion resistance of HP-Mg was dramatically upgraded by microalloying with Sc. The corrosion rates, measured by weight loss values after room-temperature immersion in a 0.6 M NaCl solution for two weeks, were found to be 0.27 and 4.0 mm y^{-1} for the HP-Mg samples with and without microalloyed 0.05wt% Sc, respectively. This improvement of the corrosion resistance due to Sc microalloying was attributed to the formation of less noble $ScFeSi_2$ particles instead of nobler Fe_3Si particles, thereby reducing susceptibility to microgalvanic corrosion as well as enhancing the integrity of the passive layer in the corrosive condition.

Acknowledgment

This work was supported by the National Research Foundation of Korea (NRF) grant funded by the Korea Government (MSIT) (No. 2019R1A2C1003905).

Supplementary materials

Supplementary material associated with this article can be found, in the online version, at doi:10.1016/j.jma.2022.08.003.

References

[1] M.S. El-Basiouny, A.A. Mazhar, Corrosion 38 (5) (1982) 237–240.
[2] J. Pouilleau, D. Devilliers, F. Garrido, S. Durand-Vidal, E. Mahé, Mater. Eng. Sci. B 47 (1997) 235–243.
[3] J.R. Davis, in: ASM Specialty Handbook, ASM International, Materials Park, Ohio, 1993, pp. 351–416.
[4] H. Ezuber, A. El-Houd, F. El-Shawesh, Mater. Des. 29 (2008) 801–805.
[5] C. Vargel, in: Corrosion of Aluminum, 2nd ed., Elsevier, Amsterdam, 2020, pp. 91–111.
[6] C.O.A. Olsson, D. Landolt, Electrochim. Acta 48 (2003) 1093–1104.
[7] B.O. Elfström, Mater. Sci. Eng. 42 (1980) 173–180.
[8] Z. Xia, K.C. Chou, Z. Szklarska-Smialowska, Corrosion 45 (8) (1989) 636–642.
[9] D. de la Fuente, I. Díaz, J. Simancas, B. Chico, M. Morcillo, Corros. Sci. 53 (2011) 604–617.
[10] G.L. Song, A. Atrens, Adv. Eng. Mater. 5 (2003) 837–858.
[11] M. Esmaily, J.E. Svensson, S. Fajardo, N. Birbilis, G.S. Frankel, S. Virtanen, R. Arrabal, S. Thomas, L.G. Johansson, Prog. Mater. Sci. 89 (2017) 92–193.
[12] J.E. Gray, B. Luan, J. Alloy. Compd. 336 (2002) 88–113.
[13] X.B. Chen, M.A. Easton, N. Birbilis, H.Y. Yang, T.B. Abbott, G.L. Song, in: Corrosion Prevention of Magnesium Alloys, Woodhead Publishing, Cambridge, 2013, pp. 282–312.
[14] H. Ardelean, I. Frateur, P. Marcus, Corros. Sci. 50 (2008) 1907–1918.
[15] G.L. Song, Z. Shi, Corros. Sci. 85 (2014) 126–140.
[16] B. Mingo, R. Arrabal, M. Mohedano, Y. Llamazares, E. Matykina, A. Yerokhin, A. Pardo, Appl. Surf. Sci. 433 (2018) 653–667.
[17] S. Hasanbeigi, S.H. Tabaian, S. Yazdani, Met. Mater. Int. 27 (2021) 4441–4454.

[18] A.S. Gnedenkov, S.V. Lamaka, S.L. Sinebryukhov, D.V. Mashtalyar, V.S. Egorkin, I.M. Imshinetskiy, M.L. Zheludkevich, S.V. Gnedenkov, Corros. Sci. 182 (2021) 109254.
[19] H. Zhu, X. Li, X. Guan, Z. Shao, Met. Mater. Int. 27 (2021) 3975–3982.
[20] G. Zhang, E. Jiang, L. Wu, W. Ma, H. Yang, A. Tang, F. Pan, Sci. Rep. 11 (2021) 2774.
[21] D. Calderón, Y. Galindez, L. Toro, A.A. Zuleta, A. Valencia-Escobar, P. Chacón, E. Correa, F. Echeverría, Met. Mater. Int. 28 (2022) 657–665.
[22] X. Zhou, Y. Huang, Z. Wei, Q. Chen, F. Gan, Corros. Sci. 48 (2006) 4223–4233.
[23] R. Arrabal, A. Pardo, M.C. Merino, M. Mohedano, P. Casajús, K. Paucar, G. Garcés, Corros. Sci. 55 (2012) 301–312.
[24] R. Jia, M. Zhang, L. Zhang, W. Zhang, F. Guo, J. Alloy. Compd. 634 (2015) 263–271.
[25] H.Y. Ha, H.J. Kim, S.M. Baek, B. Kim, S.D. Sohn, H.J. Shin, H.Y. Jeong, S.H. Park, C.D. Yim, B.S. You, J.G. Lee, S.S. Park, Scr. Mater. 109 (2015) 38–43.
[26] P. Metalnikov, G. Ben-Hamu, Y. Templeman, K.S. Shin, L. Meshi, Mater. Charact. 145 (2018) 101–115.
[27] B. Mingo, R. Arrabal, M. Mohedano, C.L. Mendis, R. del Olmo, E. Matykina, N. Hort, M.C. Merino, A. Pardo, Mater. Des. 130 (2017) 48–58.
[28] S.M. Baek, J.S. Kang, H.J. Shin, C.D. Yim, B.S. You, H.Y. Ha, S.S. Park, Corros. Sci. 118 (2017) 227–232.
[29] Z. Yin, Y. Chen, H. Yan, G. Zhou, X. Wu, Z. Hu, J. Alloy. Compd. 783 (2019) 877–885.
[30] D. Lee, B. Kim, S. Lee, S.M. Baek, J.C. Kim, H.T. Son, J.G. Lee, K.S. Lee, S.S. Park, Scr. Mater. 163 (2019) 125–129.
[31] S.M. Baek, S.Y. Lee, J.C. Kim, J. Kwon, H. Jung, S. Lee, K.S. Lee, S.S. Park, Corros. Sci. 178 (2021) 108998.
[32] J. Kwon, S.M. Baek, H. Jung, J.C. Kim, S.Y. Lee, S.S. Park, Corros. Sci. 185 (2021) 109425.
[33] S.K. Woo, C. Blawert, K.A. Yasakau, S. Yi, N. Scharnagl, B.C. Suh, Y.M. Kim, B.S. You, C.D. Yim, Corros. Sci. 166 (2020) 108451.
[34] Q. Ran, H. Yan, J. He, N. Li, Y. Lei, Met. Mater. Int. 28 (2022) 2012–2022.
[35] M. Deng, L. Wang, D. Hoche, S.V. Lamaka, C. Wang, D. Snihirova, Y. Jin, Y. Zhang, M.L. Zheludkevich, Mater. Horiz. 8 (2021) 589–596.
[36] F. Cao, Z. Shi, J. Hofstetter, P.J. Uggowitzer, G. Song, M. Liu, A. Atrens, Corros. Sci. 75 (2013) 78–99.
[37] L. Yang, G. Liu, L. Ma, E. Zhang, X. Zhou, G. Thompson, Corros. Sci. 139 (2018) 421–429.
[38] S. Fajardo, G.S. Frankel, Electrochim. Acta 165 (2015) 255–267.
[39] S.K. Woo, B.C. Suh, H.S. Kim, C.D. Yim, Corros. Sci. 184 (2021) 109357.
[40] N. Birbilis, G. Williams, K. Gusieva, A. Samaniego, M.A. Gibson, H.N. McMurray, Electrochem. Commun. 34 (2013) 295–298.
[41] R.L. Liu, J.R. Scully, G. Williams, N. Birbilis, Electrochim. Acta 260 (2018) 184–195.
[42] C. Zhang, L. Wu, H. Liu, G. Huang, B. Jiang, A. Atrens, F. Pan, Corros. Sci. 174 (2020) 108831.
[43] P. Zhao, T. Xie, T. Ying, H. Zhu, X. Zeng, Metall. Mater. Trans. A 53 (2022) 741–746.
[44] T. Xie, P. Zhao, Y. Chen, M. Zhang, Y. Wang, T. Ying, H. Zhu, X. Zeng, Mater. Charact. 179 (2021) 11294.
[45] G. Williams, H.N. McMurray, J. Electrochem. Soc. 155 (7) (2008) C340–C349.
[46] G. Williams, R. Grace, Electrochim. Acta 56 (2011) 1894–1903.
[47] W. Liu, F. Cao, Y. Xia, L. Chang, J. Zhang, Electrochim. Acta 132 (2014) 377–388.